Communication

Thermoelectric Methylene Blue Degradation by SnSe-Doped Low-Content Copper

Kaili Wang [1], Li Fan [2], Hongliang Zhu [2], Hao Liu [1], Yuxuan Wang [3] and Shancheng Yan [1,*]

1   School of Integrated Circuit Science and Engineering, Nanjing University of Posts and Telecommunications, Nanjing 210023, China; 1222228419@njupt.edu.cn (K.W.); 2023221102@njupt.edu.cn or 1021173615@njupt.edu.cn (H.L.)
2   School of Materials Science and Engineering, Nanjing University of Posts and Telecommunications, Nanjing 210023, China; 1221066836@njupt.edu.cn (L.F.); 1221066837@njupt.edu.cn (H.Z.)
3   School of Electronic Science and Engineering, Nanjing University, Nanjing 210093, China; yuhsuan605@foxmail.com
*   Correspondence: yansc@njupt.edu.cn

Abstract: In important applications, thermoelectric technology has been widely applied for precise temperature control in intelligent electronics. This work synthesized and characterized low-content copper-doped SnSe thermoelectric catalysts using an easy and effective hydrothermal method. It was discovered that doping increased the crystal plane spacing of SnSe, increased the carrier concentration, and improved the thermoelectric properties. The best degradation was attained at x = 0.0025. The thermoelectric degradation performance of low-dose copper-doped tin selenide $Sn_{1-x}Cu_xSe$ (x = 0, 0.0005, 0.001, 0.0015, 0.002, 0.0025, 0.003), for the degradation of methylene blue from organic wastewater at 75 °C, was examined. Our research indicates that by using this approach, we can create more high-performance catalysts.

Keywords: thermoelectric effect; SnSe; dopant; degradation; methylene blue

1. Introduction

Tin sulfur compounds have excellent properties and potential applications due to its thermoelectric and catalytic properties, and tin selenide, a thermoelectric material in tin sulfur compounds, has attracted much attention because of its lack of a negative impact on public health and its environmental protection benefits [1–4]. Tin selenide, a two-dimensional layered semiconductor material family member, is found in abundance in the Earth's elemental composition. It is an exceptional thermoelectric material, characterized by its high thermoelectric conversion efficiency. Notably, it possesses high electrical conductivity, while maintaining an impressively low level of thermal conductivity [5–8]. Its excellent thermoelectric properties mainly stem from its ultra-low thermal conductivity, due to its strong anharmonic and anisotropic bonding. The conversion efficiency of thermoelectric materials is determined by the thermoelectric figure of merit, $ZT = S^2\sigma T/\kappa$, where S, σ, T, and κ are the Seebeck coefficient, electrical conductivity, absolute temperature, and thermal conductivity, respectively [9–16]. It is difficult to significantly enhance $S^2\sigma$ by simply improving one of the parameters.

Moreover, the complex interrelationships between these thermoelectric parameters make it difficult to obtain high ZT values, for e.g., lower carrier concentrations lead to more significant Seebeck coefficients, but are detrimental to conductivity; larger effective masses (m*) may increase the Seebeck coefficients, but decrease carrier mobility, which leads to lower conductivity. Increasing the material's power factor (S2σ) and thermoelectric properties is necessary. Both of these aspects are closely related to the carrier concentration of the material, so continuously improving the carrier concentration is one of the most feasible ways to improve the thermoelectric merit value of the material, and doping the

material is one of the effective means to do so [17,18]. In 2015, Shi and Kioupakis et al. [15] proposed the introduction of hole doping to improve the thermoelectric properties of SnSe; Chen [19] and Leng et al. [20] proposed Ag as a dopant for SnSe; Qian [21] and Wei et al. [22] proposed Na as a dopant for SnSe, with both obtaining high ZT values; much effort has been put into regulating the carrier concentration of SnSe [23–26]. Copper and silver belong to the same group, so they can also be used as dopants for SnSe [27]. In the work of previous generations, Gong [28], Li [29], and Ghuzlan Sarhan Ahmed et al. [30], proposed enhancing the thermoelectric properties of tin selenide with copper doping up to 1%–7%. Unlike them, we dope with less copper.

In this work, we draw on the method proposed by Zhao et al. [31] to introduce trace amounts of copper into SnSe to enhance its thermoelectric properties. SnSe crystals doped with a small amount of copper were synthesized using a simple hydrothermal method, and the copper doping occupied the Sn vacancies that initially existed in SnSe, which effectively regulated the crystal structure, while increasing the hole carrier concentration. As the doping concentration slowly increases, the carrier migration first increases and then decreases, and the excess Cu occupies Sn vacancies, replaces Sn in the lattice, and strongly scatters the carriers. It was applied to wastewater treatment, and the thermal degradation of methylene blue was carried out with low-dose copper-doped SnSe at 75 °C. It was found that the concentration of methylene blue was significantly reduced after doping.

2. Materials and Methods

2.1. Materials Synthesis

All chemicals used in this experiment were of analytical grade. We synthesized $Sn_{1-x}Cu_xSe$ (x = 0, 0.0005, 0.001, 0.0015, 0.002, 0.0025) using 99.999% SeO_2 (Aladdin Reagent (Shanghai) Co., Ltd., Shanghai, China), $SnCl_2$ (Sinopharm Group Chemical Reagent Co., Ltd., Shanghai, China), and $CuCl_2$ (Shanghai Xinbao Fine Chemical Factory, Shanghai, China); the molar ratio of SeO_2 and $SnCl_2$ was 1.2:1.

SeO_2 was dissolved in ethylene glycol (Sinopharm Chemical Reagent Co., Ltd.), and then after dissolving stannous chloride dihydrate in deionized water, sodium hydroxide (Aladdin Reagent (Shanghai) Co., Ltd., China) was added to dissolve it thoroughly. Different molar masses (0%, 0.05%, 0.1%, 0.15%, 0.2%, 0.25% and 0.3%) of copper chloride were added to the $SnCl_2$ solution. The $SnCl_2$ solution was then transferred to the SeO_2 solution and mixed by thorough stirring, into which hydrazine hydrate (Sinopharm Chemical Reagent Co., Ltd.) was slowly dripped and, after stirring, the whole solution was transferred into a stainless-steel reactor lined with polytetrafluoroethylene, and was reacted for 12 h at 180 °C. The solution obtained in the reactor was centrifuged and washed, then dried to obtain a black solid powder, $Sn_{1-x}Cu_xSe$ (x = 0, 0.0005, 0.001, 0.0015, 0.002, 0.0025, 0.003). The methylene blue (Ron Reagent) solution was configured at a 45 mg/L concentration.

2.2. UV Absorption Spectrum Test

The UV absorption spectrum of the methylene blue solution was measured using a UV spectrophotometer (Shanghai Wangwan Technology, Shanghai, China, TU 1810). A total of 10 mL of the configured methylene blue solution was placed in a glass vial to which 10 mg of $Sn_{1-x}Cu_xSe$ (x = 0, 0.0005, 0.001, 0.0015, 0.002, 0.0025, 0.003) powder was added. It was then put into an oil bath at 75 °C, with stirring, and 300 µL was taken out into a cuvette every 15 min to measure the UV absorption spectrum.

2.3. Characterization

The crystal structure and morphology of the final products were characterized using X-ray diffraction (XRD, Phillips X-Pert Pro Panalytical, k = 1.540598 Å, PANalytical Co., Ltd., Almelo, The Netherlands), scanning electron microscopy (SEM, FEG Zeiss Supra 55, Zeiss Co., Ltd., Oberkochen, Germany), and transmission electron microscopy (FEI Tecnai G2 30 UT, 300 KV, FEI Co., Ltd., Hillsboro, OR, USA), respectively.

3. Results and Discussion

SnCl$_2$ was used as the Sn source, SeO$_2$ as the Se source, and copper chloride was used to provide copper ions. Sn and Se had a molar ratio of 1.2:1. Distilled water and ethylene glycol were used as solvents, and NaOH as pH adjuster. Sn$_{1-x}$Cu$_x$Se (x = 0, 0.0005, 0.001, 0.0015, 0.002, 0.0025, 0.003) crystals were synthesized using a simple and efficient hydrothermal method [32]. Throughout the synthesis process, SnCl$_2$ was a source of Sn and a reducing agent.

The powder X-ray diffractograms of the Sn$_{1-x}$Cu$_x$Se (x = 0, 0.0005, 0.001, 0.0015, 0.002, 0.0025, 0.003) samples are shown in Figures 1 and A1. After doping, all the samples showed the Pnma space group and the orthogonal structure of SnSe (JCPDS 48-1224), with an obvious peak shape indicating high crystallinity [33]. To observe the XRD pattern more clearly, we enlarged a part of it, and through the enlarged XRD pattern, we saw that the XRD peaks shifted at a low angle at x = 0.0025, which is also the case under Vegard's law [34]. The cell parameters of 0.25 wt% Cu-doped SnSe were a = 11.50376 Å, b = 4.15423 Å, and c = 4.43174 Å, whereas for pure SnSe, they were a = 11.48467 Å, b = 4.14859 Å, and c = 4.44 Å (as shown in Table 1), which indicates that the cell parameters of SnSe became larger after doping and the crystal plane spacing became larger. Elemental analysis of the samples (Figure 1c) showed that all the elements (Cu, Sn, and Se) were uniformly distributed. X-ray diffraction and elemental analysis showed successful Cu doping into the SnSe lattice. In addition, we also calculated the bandgap of SnSe and Cu-doped SnSe (as shown in Figure 1d). An estimation of the optical bandgap can be calculated by the following equation:

$$A = \frac{K\left(hv - E_g\right)^{m/2}}{hv}$$

where *A* is the absorbance, *K* is a constant, and *m* = 1 stands for the direct transition, and *m* = 2 for the indirect transition. We found that the bandgap becomes narrower with an increase in the doping concentration. The bandgap was the narrowest at a doping concentration of 0.25 wt%, and as the bandgap became narrower, the concentration of its intrinsic carriers increased, which made its electrical conductivity better.
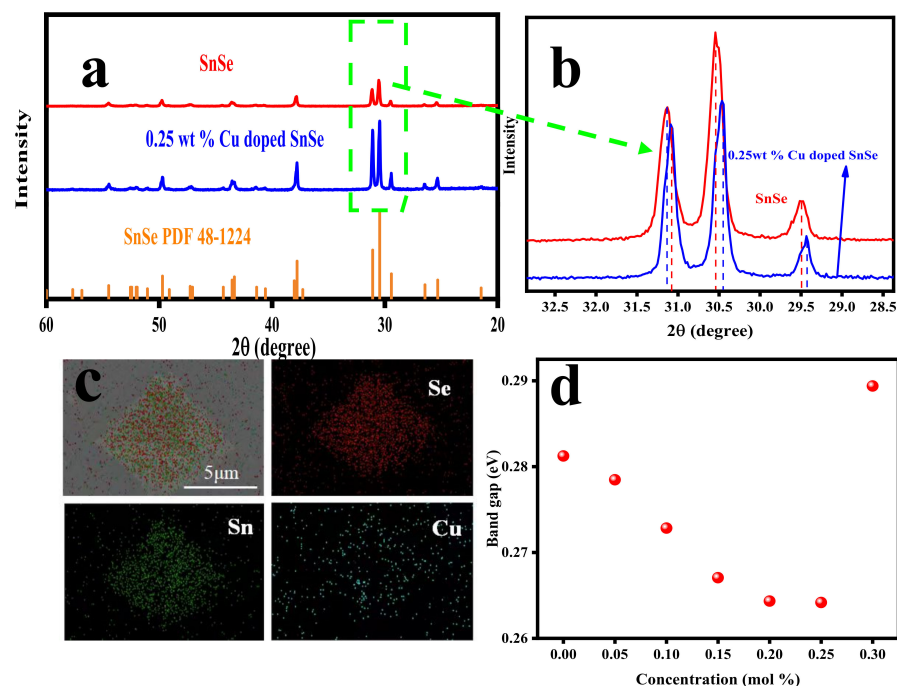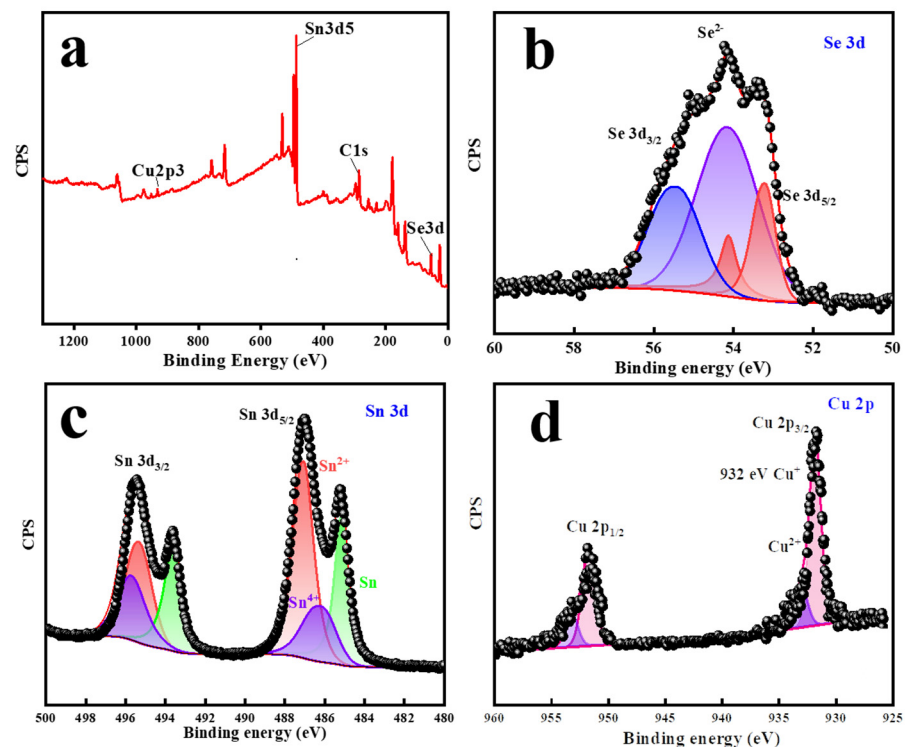

Figure 1. (**a**) X-ray diffraction (XRD) pattern of SnSe. (**b**) Enlarged view of the boxed region of the XRD pattern. (**c**) Elemental distribution diagram of SnSe. (**d**) Bandgap of SnSe and copper-doped SnSe.

Table 1. Lattice parameters of SnSe correspond to different copper-doping concentrations.

wt%	a (Å)	b (Å)	c (Å)
0	11.48467	4.14859	4.44
0.05	11.4976	4.1533	4.43976
0.1	11.50171	4.15472	4.43963
0.15	11.50255	4.15343	4.43935
0.2	11.50305	4.1538	4.43827
0.25	11.50376	4.15423	4.43175

The synthesized SnSe powder was analyzed using X-ray photoelectron spectroscopy (XPS) to investigate the valence states of copper atoms in copper-doped SnSe (as shown in Figure 2). Figure 2a shows a full spectral scan of the 0.25 wt% Cu-doped SnSe, indicating the presence of Sn 3d, Se 3d, and Cu 2p energy states. In order to explore the information about the specific energy states of these elements, Figure 2b–d shows the high-resolution scans of the XPS spectra, from which we can see that Se has only one valence state, while Sn has three valence states. Figure 2b shows the binding energy peak located at 53.7 eV, indicating that only Se-3d is present in the sample, and Figure 2c shows that Sn3d includes three valence states, Sn^{4+}, Sn^{2+}, and Sn, with Sn^{2+} being the most predominant and dominant, suggesting that the main phase in the sample is SnSe with a small amount of $SnSe_2$. In addition, as shown in Figure 2d, the binding energy peak located at 932 eV is consistent with $Cu2p_{3/2}$. Further indicating the successful doping of Cu. In addition, no significant fluctuations were found around 940–945 eV, and the presence of other Cu can also be ruled out.

Figure 2. (**a**) Survey scan of XPS spectrum for synthesized powders of 0.25 wt% Cu-doped SnSe. High-resolution scans of XPS spectra for: (**b**) Se 3d, (**c**) Sn 3d, and (**d**) Cu 2p.

As shown in Figures 3 and A2, the SEM images show the layered microstructure of SnSe crystals. With the increase in the doping concentration, the SnSe transformed from a nanoflower laminar structure to an irregular laminar structure, and the layers became thinner. The doping concentration of 0.25% resulted in the formation of a laminar structure with a rougher surface, which was more favorable for the contact with methylene blue,

and the roughened surface feature enhanced the absorption of methylene blue dye and its thermal catalytic performance.
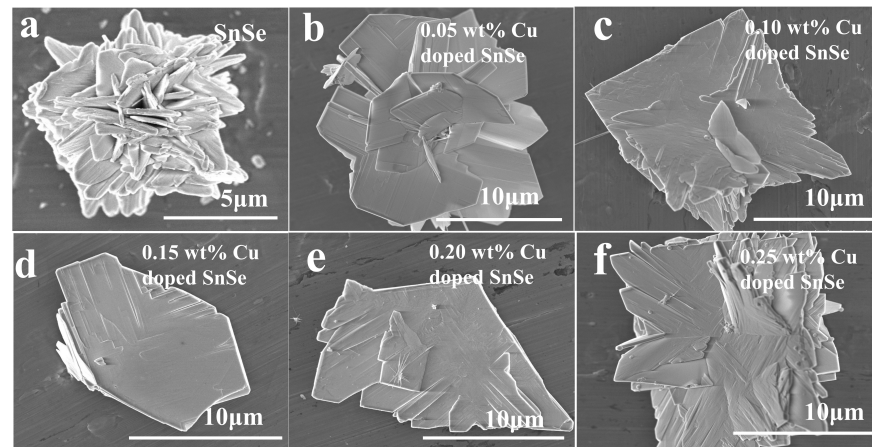

Figure 3. (**a**) SEM images of pure SnSe, (**b**) SEM images of 0.05 wt% Cu-doped SnSe, (**c**) SEM images of 0.1 wt% Cu-doped SnSe, (**d**) SEM images of 0.15 wt% Cu-doped SnSe, (**e**) SEM images of 0.2 wt% Cu-doped SnSe, and (**f**) SEM images of 0.25 wt% Cu-doped SnSe.

In order to further confirm the microstructure of SnSe and post-doped crystals, SnSe and 0.25% Cu-doped SnSe crystals were analyzed by TEM, respectively (Figure 4). By comparing Figures 4a and 4c, we can see that the SnSe crystals change from an irregular polygonal shape to a more regular rectangular structure again, which echoes the SEM images, and the edges become thinner after doping. The crystal structure is further confirmed by HRTEM, which shows that the sample exhibits clear lattice stripes. We measured the stripe spacing and found that the average spacing in the doped sample expanded from 0.28 nm to 0.29 nm, 3.5% of the spacing expansion was obvious, which indicates the success of the Cu doping, and this is in agreement with the results of the XRD.
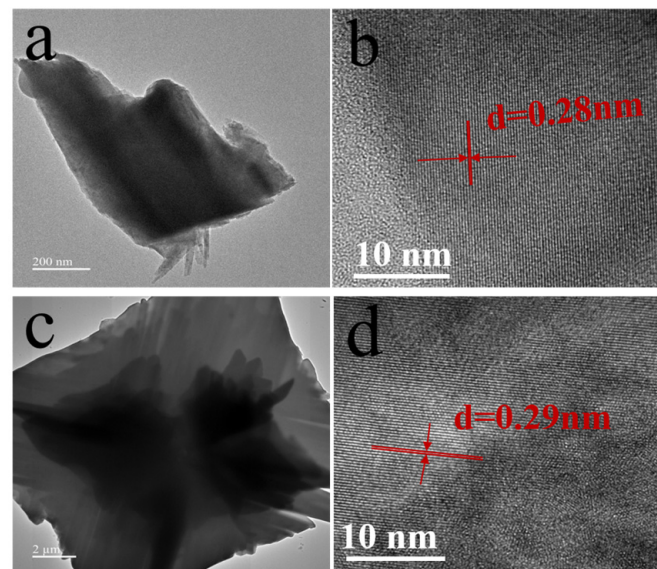

Figure 4. (**a**) TEM image of SnSe crystal. (**b**) HRTEM image of SnSe crystal. (**c**) TEM image of 0.25 wt% Cu-doped SnSe crystal. (**d**) HRTEM image of 0.25 wt% Cu-doped SnSe crystal.

Thermal degradation experiments were then carried out, as shown in Figures 5a and A3, where the UV absorption spectra of SnSe and methylene blue solutions with different Cu-doped concentrations were measured. It is seen that the concentration of the mixed solution of methylene blue and SnSe gradually decreases with the increase in the doping

concentration at 75 °C, and the best degradation effect is achieved at a doping concentration of 0.25%. To explain this phenomenon, we measured the voltage changes in SnSe and Cu-doped SnSe at different temperatures, as shown in Figure 5b. However, measuring the voltage of SnSe directly using a nanoscale was challenging. We used a 1 cm × 5 cm silicon wafer as a substrate, spread 10 g SnSe powder evenly on the substrate, covered the powder with a slide, and pressed it firmly to obtain a uniform, dense SnSe film. After that, we placed two copper electrodes at both ends of the film and fixed them with PDMS to obtain a simple SnSe device. To create a temperature gradient in the SnSe device, we put one end of the device on the heating table for about 1 min to reach the target temperature, and immediately took the device to the probe table, and used the probe to make contact with the two copper electrodes, respectively, to test the voltage at both ends. Because SnSe has good thermoelectric properties, there will be strong potential at both ends of the device, and it is obvious that the thermoelectric voltage increases with the increase in the temperature difference. Due to copper's extremely low thermoelectric coefficient, the potential that can be measured is attributed to the SnSe thermoelectric effect. Cu doping enhances the carrier concentration [28], and introducing copper can suppress carrier mobility (μ).
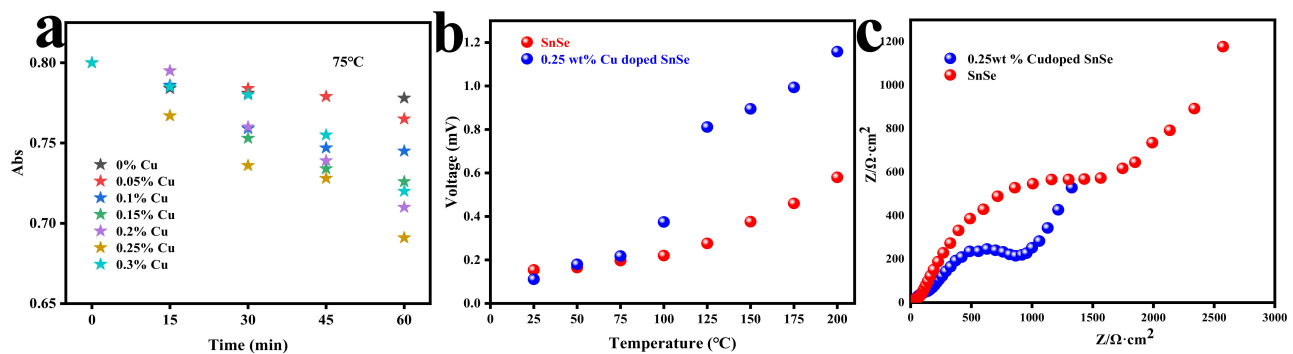

Figure 5. (**a**) Degree of degradation of methylene blue in Cu-doped SnSe with different concentrations of Cu at 75 °C. (**b**) Measurements concerning the relationship between voltage and temperature. (**c**) Impedance plots of SnSe and 0.25 wt% Cu-doped SnSe.

Moreover, the carrier mobility decreased after the first increase, because the extra copper occupies the Sn vacancies in the SnSe and replaces some Sn, weakening the scattering caused by the defects, thus increasing the carrier mobility. As the copper content increases, copper becomes predominantly doped to increase the hole carrier concentration. The subsequent decrease in carrier mobility may be because the additional Cu becomes interstitial atoms, strongly scattering the carriers and enhancing the thermoelectric properties of SnSe and, thus, resulting in a higher thermoelectric voltage. We also measured pure SnSe and 0.25 wt% impedance plots for further verification. The 0.25 wt% Cu-doped SnSe, as shown in Figure 5c, clearly shows that the resistance of the doped samples becomes smaller and the conductivity becomes more significant, again proving that the thermoelectric properties improve. Furthermore, this increase in the efficiency of degrading methylene blue stems from the thermoelectric effect of SnSe. With constant stirring of the methylene blue during the test, the temperature of the solution converged rapidly, and the extremely low thermal conductivity of SnSe made the SnSe nanoparticles unable to keep up with the temperature rise of the solution, thus creating a temperature difference. As the temperature difference increases, the concentration of electron–hole pairs and hydroxyl radicals on the surface of the SnSe increases, and the destruction rate of the methylene blue structure increases. Therefore, the degradation efficiency of methylene blue increases with the increase in the thermoelectric properties of doped SnSe.

4. Conclusions

Low-dose copper-doped SnSe crystal samples were synthesized using a simple and efficient hydrothermal method. The thermoelectric properties were improved by increasing

the doping concentration, which accelerated the degradation of methylene blue. The catalytic degradation of methylene blue by UV absorption spectroscopy at 75 °C was best achieved when the doping amount was 0.25%. The results suggest better thermal degradation can be obtained by doping with a small amount of copper in SnSe. Our work provides a new direction for environmentally friendly organic degradation and wastewater treatment using thermal catalytic technology.
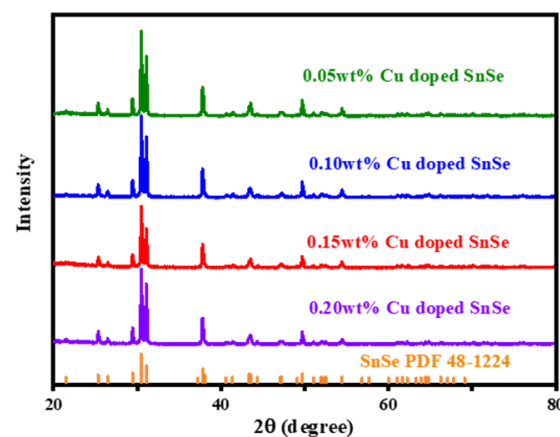
Appendix A

Figure A1. X-ray diffraction (XRD) pattern of the SnSe with different Cu doping concentrations.
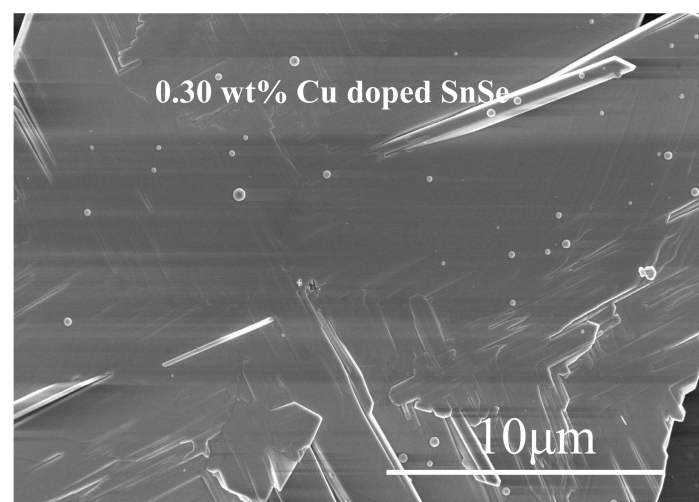

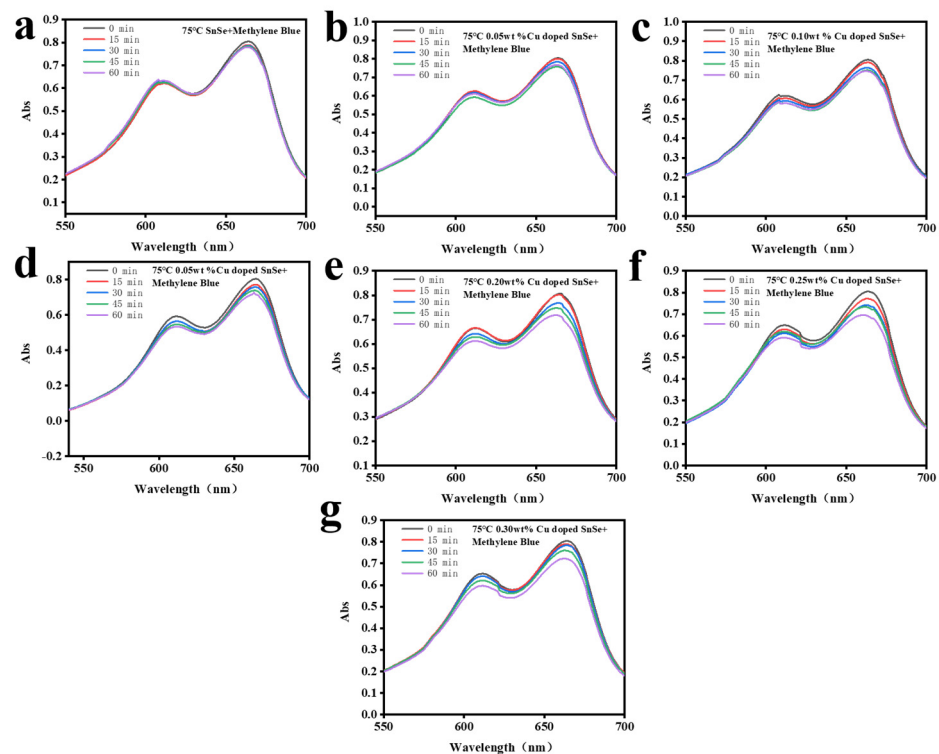**Figure A2.** SEM image of 0.30 wt.% Cu-doped SnSe.

Figure A3. (**a–g**) Variation in the UV absorption peak of methylene blue and SnSe with different Cu doping concentrations at 75 °C.

References

1. Gao, M.R.; Xu, Y.F.; Jiang, J.; Yu, S.H. ChemInform Abstract: Nanostructured Metal Chalcogenides: Synthesis, Modification, and Applications in Energy Conversion and Storage Devices. *ChemInform* **2013**, *44*. [CrossRef]
2. Kershaw, S.; Susha, A.; Rogach, A. Narrow bandgap colloidal metal chalcogenide quantum dots: Synthetic methods, heterostructures, assemblies, electronic and infrared optical properties. *Chem. Soc. Rev.* **2013**, *42*, 3033–3087. [CrossRef] [PubMed]
3. Das, L.; Guleria, A.; Neogy, S.; Adhikari, S. Porous nanostructures of SnSe: Role of ionic liquid, tuning of nanomorphology and mechanistic studies. *RSC Adv.* **2016**, *6*, 92934–92942. [CrossRef]
4. Boscher, N.D.; Carmalt, C.J.; Palgrave, R.G.; Parkin, I.P. Atmospheric pressure chemical vapour deposition of SnSe and SnSe2 thin films on glass. *Thin Solid Film.* **2008**, *516*, 4750–4757. [CrossRef]
5. Yu, J.G.; Yue, A.S.; Stafsudd, O.M. Growth and electronic properties of the SnSe semiconductor. *J. Cryst. Growth* **1981**, *54*, 248–252. [CrossRef]
6. Zhao, L.D.; Lo, S.H.; Zhang, Y.; Sun, H.; Tan, G.; Uher, C.; Wolverton, C.; Dravid, V.P.; Kanatzidis, M.G. Ultralow thermal conductivity and high thermoelectric figure of merit in SnSe crystals. *Nature* **2014**, *508*, 373–377. [CrossRef]
7. Li, L.; Chen, Z.; Hu, Y.; Wang, X.; Zhang, T.; Chen, W.; Wang, Q. Single-Layer Single-Crystalline SnSe Nanosheets. *J. Am. Chem. Soc.* **2013**, *135*, 1213–1216. [CrossRef]
8. Subramanian, B.; Mahalingam, T.; Sanjeeviraja, C.; Jayachandran, M.; Chockalingam, M.J. Electrodeposition of Sn, Se, SnSe and the material properties of SnSe films. *Thin Solid Film.* **1999**, *357*, 119–124. [CrossRef]
9. Sootsman, J.R.; He, J.; Dravid, V.P.; Ballikaya, S.; Vermeulen, D.; Uher, C.; Kanatzidis, M.G. Microstructure and thermoelectric properties of mechanically robust PbTe-Si eutectic composites. *Chem. Mater.* **2010**, *22*, 869–875. [CrossRef]
10. Chang, C.; Tan, G.; He, J.; Kanatzidis, M.G.; Zhao, L.D. The Thermoelectric Properties of SnSe Continue to Surprise: Extraordinary Electron and Phonon Transport. *Chem. Mater.* **2018**, *30*, 7355–7367. [CrossRef]
11. Jamali-Sheini, F.; Cheraghizade, M.; Yousefi, R. Electrochemically synthesis and optoelectronic properties of Pb- and Zn-doped nanostructured SnSe films. *Appl. Surf. Sci. A J. Devoted Prop. Interfaces Relat. Synth. Behav. Mater.* **2018**, *443*, 345–353. [CrossRef]
12. Wang, X.; Liu, B.; Xiang, Q.; Wang, Q.; Shen, G. Spray-Painted Binder-Free SnSe Electrodes for High-Performance Energy-Storage Devices. *ChemSusChem* **2014**, *7*, 308–313. [CrossRef] [PubMed]
13. Bhatt, V.P.; Gireesan, K.; Desai, C.F. Electrooptic properties of polycrystalline SnSe thin films. *Cryst. Res. Technol.* **2010**, *24*, 187–192. [CrossRef]
14. Han, Y.M.; Zhao, J.; Zhou, M.; Jiang, X.X.; Li, L.F. Thermoelectric performance of SnS and SnS–SnSe solid solution. *J. Mater. Chem. A* **2015**, *3*, 4555–4559. [CrossRef]
15. Shi, G.; Kioupakis, E. Quasiparticle band structures and thermoelectric transport properties of p-type SnSe. *J. Appl. Phys.* **2015**, *117*, 065103. [CrossRef]

16. Kutorasinski, K.; Wiendlocha, B.; Kaprzyk, S.; Tobola, J. Electronic structure and thermoelectric properties of n- and p-type SnSe from first principles calculations. *Phys. Rev. B* **2015**, *91*, 205201. [CrossRef]

17. Tan, G.; Zhao, L.D.; Shi, F.; Doak, J.W.; Lo, S.H.; Sun, H.; Wolverton, C.; Dravid, V.P.; Uher, C.; Kanatzidis, M.G. High thermoelectric performance of p-type SnTe via a synergistic band engineering and nanostructuring approach. *J. Am. Chem. Soc.* **2014**, *136*, 7006–7017. [CrossRef] [PubMed]

18. Wang, X.; Xu, J.; Liu, G.; Fu, Y.; Jiang, J. Optimization of thermoelectric properties in n-type SnSe doped with BiCl3. *Appl. Phys. Lett.* **2016**, *108*, 105. [CrossRef]

19. Lin, C.L.; Chang, W.H.; Wang, C.H.; Lee, C.H.; Chen, T.Y.; Jan, F.J.; Lee, G.B. A microfluidic system integrated with buried optical fibers for detection of Phalaenopsis orchid pathogens. *Biosens. Bioelectron.* **2015**, *63*, 572–579. [CrossRef]

20. Leng, H.; Zhou, M.; Zhao, J.; Han, Y.; Li, L. Optimization of Thermoelectric Performance of Anisotropic Ag$_x$Sn$_{1-x}$Se Compounds. *J. Electron. Mater.* **2016**, *45*, 527–534. [CrossRef]

21. Zhang, Q.; Chere, E.K.; Sun, J.; Cao, F.; Dahal, K.; Chen, S.; Chen, G.; Ren, Z. Studies on Thermoelectric Properties of n-type Polycrystalline SnSe$_{1-x}$S$_x$ by Iodine Doping. *Adv. Energy Mater.* **2015**, *5*, 1500360. [CrossRef]

22. Wei, T.R.; Wu, C.F.; Zhang, X.; Tan, Q.; Sun, L.; Pan, Y.; Li, J.F. Thermoelectric transport properties of pristine and Na-doped SnSe1-xTex polycrystals. *Phys. Chem. Chem. Phys.* **2015**, *17*, 30102–30109. [CrossRef] [PubMed]

23. Wei, T.R.; Tan, G.; Zhang, X.; Wu, C.F.; Li, J.F.; Dravid, V.P.; Snyder, G.J.; Kanatzidis, M.G. Distinct Impact of Alkali-Ion Doping on Electrical Transport Properties of Thermoelectric p -Type Polycrystalline SnSe. *J. Am. Chem. Soc.* **2016**, *138*, 8875–8882. [CrossRef] [PubMed]

24. Gharsallah, M.; Serrano-Sánchez, F.; Nemes, N.M.; Mompeán, F.J.; Martínez, J.L.; Fernández-Díaz, M.T.; Elhalouani, F.; Alonso, J.A. Giant Seebeck effect in Ge-doped SnSe. *Sci. Rep.* **2016**, *6*, 26774. [CrossRef] [PubMed]

25. Chen, Y.X.; Ge, Z.H.; Yin, M.; Feng, D.; Huang, X.Q.; Zhao, W.; He, J. Understanding of the Extremely Low Thermal Conductivity in High-Performance Polycrystalline SnSe through Potassium Doping. *Adv. Funct. Mater.* **2016**, *26*, 6836–6845. [CrossRef]

26. González-Romero, R.L.; Meléndez, J.J. Variation of the zT factor of SnSe with doping: A first-principles study. *J. Alloys Compd. Interdiscip. J. Mater. Sci. Solid-State Chem. Phys.* **2018**, *732*, 536–546.

27. Singh, N.K.; Bathula, S.; Gahtori, B.; Tyagi, K.; Haranath, D.; Dhar, A. The effect of doping on thermoelectric performance of p-type SnSe: Promising thermoelectric material. *J. Alloys Compd.* **2016**, *668*, 152–158. [CrossRef]

28. Gong, Y.; Chang, C.; Wei, W.; Liu, J.; Xiong, W.; Chai, S.; Li, D.; Zhang, J.; Tang, G. Extremely low thermal conductivity and enhanced thermoelectric performance of polycrystalline SnSe by Cu doping. *Scr. Mater.* **2018**, *147*, 74–78. [CrossRef]

29. Li, J.; Xu, J.; Wang, H.; Liu, G.-Q.; Tan, X.; Shao, H.; Hu, H.; Jiang, J. Enhanced thermoelectric performance in p-type polycrystalline SnSe by Cu doping. *J. Mater. Sci. Mater. Electron.* **2018**, *29*, 18727–18732. [CrossRef]

30. Ahmed, G.S.; Al-Maiyaly, B.K. Cu doping effect on characterization of nano crystalline SnSe thin films. *AIP Conf. Proc.* **2019**, *2190*, 020019.

31. Liu, D.; Wang, D.; Hong, T.; Wang, Z.; Wang, Y.; Qin, Y.; Su, L.; Yang, T.; Gao, X.; Ge, Z.; et al. Lattice plainification advances highly effective SnSe crystalline thermoelectrics. *Science* **2023**, *380*, 841–846. [CrossRef] [PubMed]

32. Ge, Z.H.; Wei, K.; Lewis, H.; Martin, J.; Nolas, G.S. Bottom-up processing and low temperature transport properties of polycrystalline SnSe. *J. Solid State Chem.* **2015**, *225*, 354–358. [CrossRef]

33. Guo, H.; Xin, H.; Qin, X.; Zhang, J.; Li, D.; Li, Y.; Song, C.; Li, C. Enhanced thermoelectric performance of highly oriented polycrystalline SnSe based composites incorporated with SnTe nanoinclusions. *J. Alloys Compd.* **2016**, *689*, 87–93. [CrossRef]

34. Denton, A.R.; Ashcroft, N.W. Vegard's law. *Phys. Rev. A At. Mol. Opt. Phys.* **1991**, *43*, 3161. [CrossRef] [PubMed]